The signal demodulation techniques

Yassine Amirat, Mohamed Benbouzid

The signal demodulation techniques

Yassine Amirat[1] and Mohamed Benbouzid[2]

Condition monitoring of electrical machines is a broad scientific area, the ultimate purpose of which is to ensure the safe, reliable and continuous operation of electrical machines. Hence, the task of fault detection is still an art, because induction machines are widely used in variable speed drives and in renewable energy conversion systems. A deep knowledge about all the phenomena involved during the occurrence of a failure constitutes an essential background for the development of any failure detection and diagnosis system. For the failure detection problem, it is important to know if a failure exists or not in the electric machine via the processing of available measurements. This chapter provides then an approach based on a electric machine current data collection and attempts to highlight the use of demodulation techniques for failure detection for stationary and nonstationary cases.

2.1 Introduction

Electrical machines have become unavoidable device in industrial and domestic applications, for producing mechanical power in drive trains or transforming it into electrical power in generation systems. So, it is to be expected that electrical machines are related to huge financial variables as well as safety and reliability. Despite electrical machines are robust devices, they remain subject to faults and downtime, hence, affecting their reliability performances. According to the defected component and the type of the electrical machine, faults can be classified in three categories:

- Stator-related fault: It includes electrical failures affecting the stator winding such as short circuits, inter-turn short circuits and open circuits [1].
- Rotor-related fault: It includes electrical failures affecting the rotor winding, commutators/slip rings/brushes failures for all rotor-wounded machines, and broken rotor bars and end rings for squirrel-cage machines, and permanent magnet demagnetization or cracks for permanent magnet motors.
- Mechanical-related fault: It includes bearing failures, rotor eccentricity and shaft misalignment.

[1]ISEN Yncréa Ouest, LABISEN, Brest, France
[2]Institut de Recherche Dupuy de Lôme, CNRS, University of Brest, Brest, France

The safety and reliability of electrical machines are related directly to these faults, hence affecting the operation and maintenance cost. So, new challenges arise particularly with regard to maintenance. In this context, cost-effective, predictive and proactive maintenance assume more importance. Condition monitoring systems (CMS) provide then an early indication of component incipient failure, allowing the operator to plan system repair prior to complete failure. Hence, CMS will be an important tool for lifting uptime and maximizing productivity, when cost-effective availability targets must be reached.

For this purpose, many techniques and tools are developed for condition monitoring of electrical machines in order to prolong their life span as reviewed in [2]. Some of the technologies used for monitoring include existing and pre-installed sensors, such as speed sensor, torque sensor, vibrations, temperature and flux density sensor. These sensors are managed together in different architectures and coupled with algorithms to allow an efficient monitoring of the system condition. A plethora of electrical machines faults and diagnostic methods are presented in the literature. The most favorable is the motor current signature analysis (MCSA) which is the analysis of the stator current harmonics index [3,4]. Most define the MSCA as the monitoring and spectra analysis of the stator current at steady state. Despite the method's origins, the name is very generic and should include the analysis of the stator current spectra under transient operation also. Anyway, this method has become favorable due to its unique characteristics such as remote monitoring [5], low implementation costs and equipment, and continuous and online monitoring capability. The advantage of signature analysis of the motor electrical quantities is that it is a noninvasive technique as those quantities are easily accessible during operation [6]. Moreover, stator currents are generally available for other purposes such as control and protection, avoiding the use of extra sensors [7]. Hence, most of the recent researches on induction machine faults detection have been focused on electrical monitoring with emphasis on current analysis [8,9].

Industrial survey on condition monitoring of induction motors show important features of failure rate and index the major faults of electrical machines can broadly be classified by the following [2,10]:

- Static and/or dynamic air-gap irregularities
- Broken rotor bar or cracked rotor end-rings
- Stator faults (opening or shorting of one coil or more of a stator phase winding)
- Abnormal connection of the stator windings
- Bent shaft (akin to dynamic eccentricity) which can result in a rub between the rotor and stator, causing serious damage to stator core and windings
- Bearing and gearbox failures.

The most common faults are bearing faults, stator faults, rotor faults and eccentricity or any combination of these faults. When analyzed statistically, about 40% of the faults correspond to bearing faults, 30–40% to stator faults, 10% to rotors faults, while remaining 10% belong to a variety of other faults. Frequencies induced by each fault depend on the particular characteristic data of the motor (like synchronous speed, slip frequency and pole-pass frequency) as well as operating conditions.

Moreover, in many industries context, bearing failures have been a persistent problem which accounts for a significant proportion of all failures in electrical machines; for example, bearing failure of electric drive or rotating electric generation system is the most common failure mode associated with a long downtime. Bearing failure is typically caused by improper lubrication, and occasionally manufacturing faults in the bearing components, and also some misalignment in the drive train, which gives rise to abnormal loading and accelerates bearing wear. A plethora of research works [11,12] states that due to the construction of rolling-element bearings, a defect generates precisely identifiable signature on vibration, and the generated frequencies present an effective route for monitoring progressive bearing degradation. On the other hand, experience and industrial feedback have demonstrated that vibration monitoring has made out its efficiency; and it is highly suitable for rolling-element bearings—however it represents an issue when requiring a good vibration baseline [13]. If no baseline is available, no history has been built up, making the detection of the specific frequencies impossible when the background noise has risen [12].

To overcome this issue, many alternatives have emerged in electric machines by analyzing the stator-side electrical quantities. These alternatives are known as MCSA, including the use of electrical current [13,14], or the instantaneous power factor [15]. For steady-state operations, current spectral estimation based on fast Fourier transform (FFT) and its extension, the short-time Fourier transform (STFT), have been widely employed, such as FFT-based bispectrum/bicoherence [9]. Due to frequency limitation of these techniques [16], high resolution technique: MUSIC (MUltiple SIgnal Classification) [17] and ESPRIT (Estimation of Signal Parameters via Rotational Invariance Techniques) [18,19] were afterwards investigated. However, these techniques have several drawbacks since they are difficult to interpret and it is difficult to extract variation features in time domain for nonstationary signals. To overcome this problem and under nonstationary behavior, procedures based on time-frequency representations (spectrogram, quadratic Wigner-Ville, etc.) [20–22] or time-scale analysis (wavelet) have been proposed in the literature of the electric machines community [23–25]. There are also parametric methods based on parameter estimation of a known model [16]. Nevertheless, these methods are formulated through integral transforms and analytic signal representations [26], so their accuracy depends on data length, stationarity and model accuracy.

Most of electric machine faults lead to current modulation (amplitude and/or phase) [27]. This is the particular case of bearing faults [28]. Indeed, a bearing fault is assumed to produce an air-gap eccentricity [21], and consequently, an unbalanced magnetic pull. Hence, this gives rise to torque oscillations, which lead to amplitude and/or phase modulation of the stator current [13,21,29].

So, for failure detection, a possible approach relies on the use of amplitude demodulation techniques; in other words, the fault detection relies on the extraction of the instantaneous amplitude (IA) and/or the instantaneous frequency (IF). Therefore, it is sufficient to demodulate the current for bearing faults detection. However, the demodulation techniques depend on the type and the dimension of the signal. In this chapter, we try to highlight the use of demodulation techniques for mono-dimensional and multidimensional signals and for mono-component and multicomponent signals.

2.2 Brief status on demodulation techniques as a fault detector

As mentioned, the investigation of demodulation techniques as a failure detection relies on the extraction of the IA and/or IF of the electrical quantities, and in most cases, the machine current is taken as a transducer of the fault. For demodulation, let us consider the complex (analytic signal) representation of such signals is given by

$$x(t) = a(t)\mathrm{e}^{j\phi(t)} \tag{2.1}$$

where $a(t)$ and $\phi(t)$ are the IA and instantaneous phase, respectively. Signals with more complicated structure can be represented by a combination of signals of this type. A survey allowed to establish a road map for different demodulation techniques [30] and the choice of the demodulation technique depends on the type of the signal.

2.2.1 Mono-component and multicomponent signals

A mono-component signal is described in the time-frequency domain by one single "crest or ridge," corresponding to an elongated region of energy concentration [31,32]. Furthermore, interpreting the crest as a graph of IF versus time, the IF of a mono-component signal is a single-valued function of time. Consequently, such a mono-component signal can be expressed approximately as

$$z(t) = a(t)\cos(\phi(t)) \tag{2.2}$$

where

- $a(t)$, known as the IA, is real and positive;
- $\phi(t)$ is known as the instantaneous phase.

It will be noted that in the electrical community $z(t)$ has an analytic associate of the form given by

$$z(t) = a(t)\mathrm{e}^{j\phi(t)}. \tag{2.3}$$

A multicomponent signal may be described as the sum of two or more mono-component signals such that

$$z(t) = \sum_{n=1}^{\infty} a_i(t)\cos(\phi(t)) \tag{2.4}$$

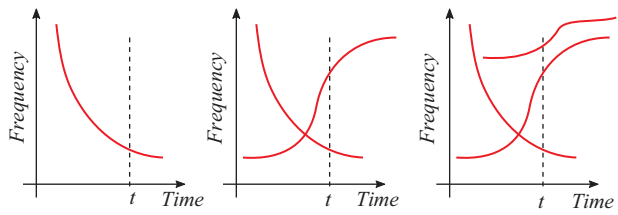

Figure 2.1 Evolution of the IF for both mono-component and multicomponent signals

The model described by (2.4) allows the extraction and separation of components from a given multicomponent signal using (t,f) filtering methods [33]. Figure 2.1 shows the evolution of the IF of a mono-component signal and multicomponent signal with two and three components.

2.2.2 Demodulation techniques

Most of electric machine faults lead to current modulation (amplitude and/or phase) [27]. This is the particular case of bearing faults [28]. So, for failure detection, a possible approach relies on the use of amplitude demodulation techniques; in other words, the fault detection relies on the extraction of the IA and IF.

2.2.2.1 Mono-dimensional techniques

As depicted in Figure 2.2, mono-dimensional techniques include synchronous demodulation, Hilbert transform (HT) and Teager–Kaiser energy operator (TKEO).

A mono-dimensional signal can be modeled in discrete form by

$$x(n) = a(n) \cdot \cos(\Phi(n)) \tag{2.5}$$

where $n = 0, \ldots, N-1$ is the sample index, with N being the number of samples. In (2.5), frequency ω is equal to $2\pi f/F_e$ (where f and F_e are the supply and sampling frequency, respectively) and amplitude $a(n)$ is related to the fault. In this context, the

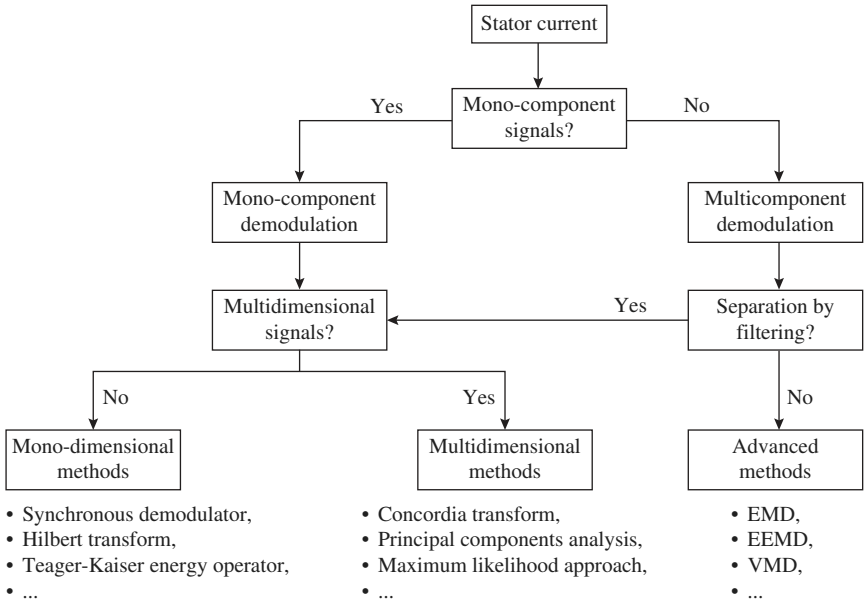

Figure 2.2 Road map to choose the demodulation technique

best path to extract feature extraction is the use of amplitude demodulation techniques. The signal $x(n)$ can be expressed in term of its IA and instantaneous phase as follows:

$$x(n) = a(n) \cdot \cos(\Phi(n)) \tag{2.6}$$

The signal $x(n)$ can be expressed in terms of two components: real component y_1 and imaginary component y_2 such as

$$y_1(n) = a(n) \cdot \cos(\Phi(n)) \qquad y_2(n) = a(n) \cdot \sin(\Phi(n)) \tag{2.7}$$

and $x(n)$ can be expressed by it is analytic signal representation as

$$x(n) = y_1(n) + jy_2(n) \tag{2.8}$$

2.2.2.2 Multidimensional techniques

In electrical systems, a multidimensional signal refers to a multiphase systems; particularly in triphase systems, signals can be modeled in discrete form by

$$x_{0,1,2}(n) = a_{0,1,2}(n) \cdot \cos(\Phi_{0,1,2}(n)) \tag{2.9}$$

For instance, we assume a three-phase system that does not contain any harmonics, but in a noisy environment. The three-phase quantities can therefore be expressed by system (2.10):

$$\begin{cases} x_0(t) = a_0 \cos(\omega t + \alpha_0) \\ x_1(t) = a_1 \cos(\omega t + \alpha_1) \\ x_2(t) = a_2 \cos(\omega t + \alpha_2) \end{cases} \tag{2.10}$$

where a_0, a_1 and a_2 are the three magnitudes, and ω is the angular frequencies, and α_0, α_1 and α_2 are the three initial phase angles of the corresponding phase.

The three-phase system can be expressed in a compact form as follows [34]:

$$x_m[k] = a_m \cos(k\omega_0 + \alpha_m) \tag{2.11}$$

where $\omega_0 = 2\pi \frac{f_0}{F_s}$ corresponds to the fundamental angular frequency, $m = 0, 1$ or 2 corresponds to the phase index for the three-phase electrical system, f_0 is the fundamental frequency, F_s is the sampling frequency, $x_0[k]$, $x_1[k]$ and $x_2[k]$ are the electric signal of each phase, and a_a, a_b, a_c, α_a, α_b and α_c are, respectively, the amplitudes and initial phases of each fundamental component of the three-phase system. Hence, the most common path to demodulate a multidimensional signal is the use the transformation of the three-phase quantities modeled by (2.11) to the corresponding complex phasor. The complex phasor for three-phase system can be expressed as follows:

$$x_m = x_\alpha + jx_\beta \tag{2.12}$$

where x_α and x_β are the direct and quadrature components obtained by the use of (abc) to $(\alpha\beta)$ transform. For multidimensional signal, the case of three-phase system, the three-phase transformations such as Concordia transform (CT) [35,36] and Park vector approach [37–39] have been indexed as a demodulation techniques.

2.3 Synchronous demodulation

Synchronous demodulation is an amplitude and phase demodulation technique. Figure 2.3 illustrates the principle of this demodulation technique, and it shows that the analyzed signal is multiplied with two reference signals F_1 and F_2.

Let a signal:

$$i(t) = a(t)\cos(2\pi f_p t + \varphi) \tag{2.13}$$

By multiplying the signal $i(t)$ by a carrier with pulsation ω_p:

$$F_1(t) = i(t)\cos(2\pi f_p t) \tag{2.14}$$

$$F_2(t) = i(t)\sin(2\pi f_p t) \tag{2.15}$$

Using the trigonometric properties, we obtain:

$$F_1(t) = (a(t)/2)(\cos(4\pi f_p t + \varphi) + \cos(\varphi)) \tag{2.16}$$

$$F_2(t) = (a(t)/2)(\sin(4\pi f_p t + \varphi) + \cos(\varphi)) \tag{2.17}$$

To simplify the mathematical analysis, we use the frequency-domain representation of F_2 and F_2; this yields to

$$F_1(f) = (a(f)/2)\left(\frac{1}{2}(\delta(f - 2f_p) + \delta(f + 2f_p)) \cdot \mathrm{e}^{jf\varphi} + \cos(\varphi)\delta(f)\right) \tag{2.18}$$

$$F_1(f) = \frac{\cos(\varphi)}{2}a(f) + \frac{\mathrm{e}^{jf\varphi}}{4}(a(f - 2f_p) + a(f + 2f_p)) \tag{2.19}$$

In the same way, it can be shown that

$$F_2(f) = (a(f)/2)\left(\frac{1}{2}(\delta(f - 2f_p) + \delta(f + 2f_p)) \cdot \mathrm{e}^{jf\varphi} + \cos(\varphi)\delta(f)\right) \tag{2.20}$$

then

$$F_2(f) = \frac{\sin(\varphi)}{2}a(f) + \frac{j \cdot \mathrm{e}^{jf\varphi}}{4}(a(f + 2f_p) - a(f - 2f_p)) \tag{2.21}$$

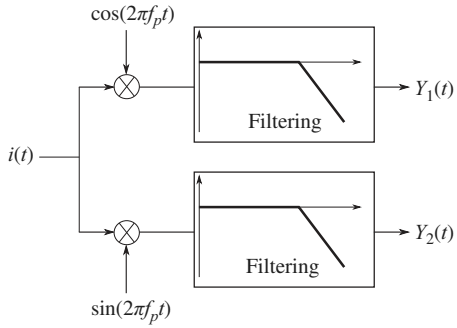

Figure 2.3 Synchronous demodulation principle

Under the assumption that the spectrum of $a(f)$ is frequency-bounded $[-f_{\max}, f_{\max}]$ with $f_{\max} < f_p$, it is possible to extract $a(f)$ with a low-pass filter of cutoff frequency f_p. Assuming that the low-pass filter is ideal (brickwall filter), the post-filter signals denoted by $F_1^{(pf)}(f)$ and $F_2^{(pf)}(f)$ can then be expressed as follows:

$$F_1^{(pf)}(f) = \frac{\cos(\varphi)}{2} a(f) \tag{2.22}$$

$$F_2^{(pf)}(f) = \frac{\sin(\varphi)}{2} a(f) \tag{2.23}$$

$$F_2^{(pf)}(f) = \frac{\sin(\varphi)}{2} a(f) \tag{2.24}$$

$$z(t) = \left(y_1^{(pf)}(t)\right)^2 + \left(y_2^{(pf)}(t)\right)^2 \tag{2.25}$$

$$z(t) = (a(t))^2 \cdot \left(\left(\frac{\cos(\varphi)}{2}\right)^2 + \left(\frac{\sin(\varphi)}{2}\right)^2\right) \tag{2.26}$$

$$z(t) = \frac{(a(t))^2}{4} \tag{2.27}$$

By this method, we can extract the IA of the signal. Except that, this approach has several drawbacks. First of all, its application requires to know exactly the frequency f_p. In particular, a poor knowledge of f_p deteriorates considerably the estimation of the IA. Second, this technique requires the selection and calibration of a low-pass filter as well as the choice of a filter structure and a perfectly adapted cutoff frequency.

Synchronous demodulation has been applied for fault detection in electrical machines running at constant speeds. However, for machines rotating at variable speeds, synchronous demodulation requires a good knowledge of the law of evolution of the IF.

2.4 Hilbert transform

In order to estimate the IF and IA of a signal, a standard approach is to use the HT. The HT is a linear operator for which analytic signals can be derived if the Bedrosian theorem is verified from the signal $x(n)$. It is defined as the convolution (*) of the signal with the function $1/t$ [40]. If $\hat{x(t)}$ is the HT of a signal $x(t)$, the analytic signal introduced by [41] is given by the following equation:

$$z(t) = x(t) + j\hat{x(t)} \tag{2.28}$$

and $\hat{x(t)}$ is expressed by

$$\hat{x(t)} = x(t) * \frac{1}{\pi t} \tag{2.29}$$

For its discrete formulation, let us consider a discrete signal $x(n)$. The discrete HT (DHT) of $x(n)$ is given by the following [42]:

$$\mathscr{H}[x(n)] = \mathscr{F}^{-1}\{\mathscr{F}\{x(n)\} \cdot u(n)\} \tag{2.30}$$

where $\mathscr{F}\{\cdot\}$ and $\mathscr{F}\{\cdot\}$ correspond to the FFT and inverse FFT (IFFT), respectively, and where $u(n)$ is defined as

$$u(n) = \begin{cases} 1, & n = 0, \frac{N}{2} \\ 2, & n = 1, 2, \ldots, \frac{N}{2} - 1 \\ 0, & n = \frac{N}{2} - 1, \ldots, N - 1 \end{cases} \tag{2.31}$$

Let us define the analytic signal of $x(n)$, denoted $z(n)$, as

$$z_k(n) = x_k(n) + j\mathscr{H}[x_k(n)] \tag{2.32}$$

Using signal model (2.5), the amplitude envelope can be estimated by [42]:

$$|a(n)| \approx |z(n)| = \sqrt{x_k(n)^2 + \mathscr{H}[x_k(n)]^2} \tag{2.33}$$

and the instantaneous phase $\phi(n)$ can be estimated by

$$\phi(n) = Arg(z(n)) \tag{2.34}$$

2.5 Teager–Kaiser energy operator

The TKEO is an IA and IF demodulation technique for mono-component signal, and it estimates IA and IF without using the analytical signal $z(n)$. The estimation of IA and IF with TEO technique is based on the continuous energy separation algorithm, given by the following [43]:

$$|a(t)| \approx \frac{\psi[x(t)]}{\sqrt{\psi[\dot{x(t)}]}} \tag{2.35}$$

$$f(t) \approx \frac{1}{2\pi}\sqrt{\frac{\psi[\dot{x(t)}]}{\psi[x(t)]}} \tag{2.36}$$

with ψ is the so-called TKEO:

$$\psi = [\dot{x(t)}]^2 - x(t)\ddot{x(t)}$$

where $x(t)$ is the analyzed signal and $\dot{x(t)}$ and $\ddot{x(t)}$ are its first and second derivatives, respectively.

It will be noted that, for discrete signals, the TKEO offers excellent time resolution because only three samples are required for the energy computation at each time instant, hence the result is highly depending on the sampling frequency. So, for discrete signals, the TKEO technique is performed by using the discrete-time

energy separation algorithm developed in [44] and well known as (DESA-2). In this algorithm, the estimated IA and IF are given using the following equations:

$$|a(n)| \approx \frac{2\psi(x(n))}{\sqrt{\psi(x(n+1)-x(n-1))}} \tag{2.37}$$

$$f(n) \approx \frac{1}{2\pi}\arccos\left(1-\frac{\psi(x(n)-x(n-1))}{2\psi(x(n))}\right) \tag{2.38}$$

where the TKEO can be approximated by time differences as follows:

$$\psi = [x(n)]^2 - x(n+1)x(n-1)$$

2.6 Concordia transform

The CT converts the three-phase current to Park's space vector components $i_\alpha(n)$ and $i_\beta(n)$, as depicted by Figure 2.4.

The Park components are given by

$$\begin{bmatrix} i_\alpha(n) \\ i_\beta(n) \end{bmatrix} = \begin{bmatrix} \frac{2}{3} & -\frac{1}{3} & -\frac{1}{3} \\ 0 & \frac{1}{\sqrt{3}} & -\frac{1}{\sqrt{3}} \end{bmatrix} \begin{bmatrix} i_0(n) \\ i_1(n) \\ i_2(n) \end{bmatrix} \tag{2.39}$$

Several fault detectors based on CT have been proposed in literature [35–37, 45–47]. Recently, it has been shown that CT can be viewed as a demodulation technique for balanced system [35]. Indeed, under the assumption that the system is balanced, the Park components can be expressed as

$$\begin{aligned} i_\alpha(n) &= a(n)\cos(\omega n) \\ i_\beta(n) &= a(n)\sin(\omega n) \end{aligned}$$

Then, the amplitude can be estimated by

$$|a(n)| = \sqrt{i_\alpha^2(n) + i_\beta^2(n)} \tag{2.40}$$

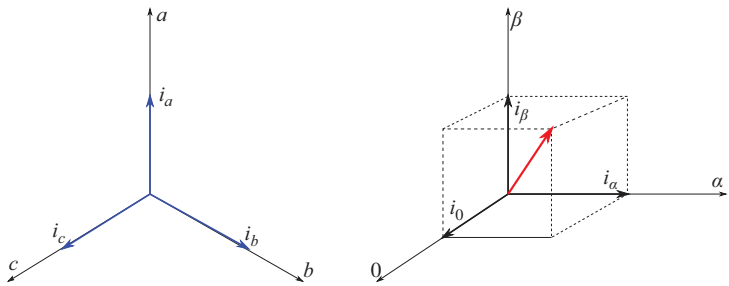

Figure 2.4 CT principle

It will be noted that for balanced system, the component i_0 is null. Therefore, CT can be considered as a low-complexity demodulating technique *if* the system is balanced. However if the system is unbalanced, and there is no assertion that during bearing fault the three-phase system remains balanced, (2.40) is no longer valid and depends on three modulating signals $i_a(n)$, $i_b(n)$ and $i_c(n)$, and the corresponding space phasor in its extended form is computed according to (2.41):

$$\vec{i}(n) = i_\alpha(n)\vec{u}_\alpha + i_\beta(n)\vec{u}_\beta + i_0(n)\vec{u}_0 \tag{2.41}$$

where i_α, i_β and i_0 are the components according to axis, respectively, and are the corresponding unit vectors, and the IA can be estimated by

$$|i(n)| = \sqrt{(i_\alpha(n))^2 + (i_\beta(n))^2 + (i_0(n))^2} \tag{2.42}$$

2.7 Fault detector

Several detectors based on the IA have been proposed in the literature [36,45,48–51]. However, most of these approaches use unnecessary and complicated classifiers, such as artificial neural networks, fuzzy logic and support vector machine, and most of them assume that a training database is available. This can be very difficult to obtain for many industrial applications. Indeed, it has been mentioned in a number of previously published papers that one of the main difficulties in real-word testing of developed condition monitoring technique is the lack of collaboration needed with industrial operators and manufacturers due to data confidentiality, particularly when failures are present [52], and can be difficult to obtain [53]. For this purpose, a statistical feature-based detector is proposed; it does not require any training sequence. The detector is based on the variance of $|a(n)|$ or $|a_k(n)|$, and the two basic parameters are the mean value μ and the standard deviation σ [54].

2.7.1 Fault detector based on HT and TKEO demodulation

After applying HT or TKEO independently on the three currents, we propose to exploit the information given by the three extracted envelopes. To avoid the edge effect problem of HT and TKEO, each envelope is truncated by removing α samples at the beginning and at the end of $|a_k(n)|$. The proposed criterion, σ_H^2 (i.e. σ_{TKEO}^2), is then equal to

$$\sigma_H^2 = \frac{1}{3(N-2\alpha)} \left(\sum_{k=0}^{2} \sum_{n=\alpha}^{N-\alpha-1} (|a_k(n)| - \mu_k)^2 \right) \tag{2.43}$$

where μ_k is the average of $|a_k(n)|$, i.e.

$$\mu_k = \frac{1}{(N-2\alpha)} \sum_{n=\alpha}^{N-\alpha-1} |a_k(n)| \tag{2.44}$$

In (2.43), the average is used to make the criteria σ_H^2, σ_{TKEO}^2 and σ_C^2 equivalent for balanced system. Indeed if $a_k(n) = a(n)$ for all $k = \{0, 1, 3\}$ and if the edge

effects problems are neglected, then it can be shown that $\sigma_H^2 = \sigma_C^2 = \sigma_{TKEO}^2$ with $\alpha = 0$. This property no longer holds for unbalanced system. For healthy unbalanced system, envelopes $a_k(n)$ are different but they are all constant. It follows that $|a_0(n)| = \mu_0$, $|a_1(n)| = \mu_1$ and $|a_2(n)| = \mu_2$ and so $\sigma_H^2 = 0$. Therefore, we propose a simple hypothesis test to detect a fault under unbalanced condition:

- If $\sigma_H^2 < \gamma_H$, the machine is healthy.
- If $\sigma_H^2 > \gamma_H$, the machine is faulty.

Here γ_H is a threshold which can be set subjectively. One should remark that this second hypothesis test is more powerful since it can be employed for balanced and unbalanced systems. In this section, the result of several simulations is presented to compare the performance of the proposed fault detectors. For each simulation, the amplitude envelope is estimated through CT, HT and TKEO. Then, depending of the demodulation technique, criteria σ_C^2, σ_H^2 or σ_{TKEO}^2 are computed to reveal the presence of a fault. The simulation has been performed for healthy and faulty machine.

2.7.2 Fault detector after CT demodulation

After applying CT, envelope $|a(n)|$ is extracted with (2.40). Then, we propose to compute the variance of $|a(n)|$ to detect a fault. This statistic criterion, denoted σ_C^2, is given by

$$\sigma_C^2 = \frac{1}{N}\sum_{n=0}^{N-1}(|a(n)| - \mu)^2 \tag{2.45}$$

where μ is the average of $|a(n)|$, i.e.

$$\mu = \frac{1}{N}\sum_{n=0}^{N-1}|a(n)| \tag{2.46}$$

The variance σ_C^2 measures the deviation of the amplitude around its mean μ. This criterion can be used to detect amplitude modulation for balanced system. Indeed, if no fault is present, $|a(n)|$ is constant and so $|a(n)| = \mu$. Using (2.63), it follows that $\sigma_C^2 = 0$. On the contrary, for healthy machine $|a(n)| \neq \mu$, which also implies $\sigma_C^2 > 0$. Therefore, we can propose a simple hypothesis test to detect a fault under balanced assumption:

- If $\sigma_C^2 < \gamma_C$, the machine is healthy.
- If $\sigma_C^2 > \gamma_C$, the machine is faulty.

Here γ_C is a threshold which can be set subjectively. For unbalanced system, one should note that this simple hypothesis test is no longer valid since σ_C^2 is not necessarily equal to 0 for healthy machine.

2.7.3 Synthetic signals

Several simulations are presented to compare the performance of the proposed fault detectors. For each simulation, the amplitude envelope is estimated through CT, HT and TKEO. Then, depending on the demodulation technique, criteria σ_C^2, σ_H^2 or σ_{TKEO}^2

are computed to reveal the presence of a fault. The simulation have been performed for healthy and faulty machine.

For this purpose, several simulations have been performed with amplitude modulated (AM) synthetic signals which are defined as follows [21]:

$$i_k(n) = \underbrace{(1 + \beta \sin(\omega_2 n + \psi_k))}_{a_k(n)} \cdot \cos(\omega n + \phi_k) \tag{2.47}$$

where β is a fault index which is equal to 0 for healthy machines and greater than 0 for faulty ones. The parameters ψ_k and γ_k are calibrated depending on the balanced assumption. If the system is balanced, $\psi_k = \psi$ $(k = 0, 1, 2)$, where ψ_k depends on k for unbalanced system. Simulations have been run with a sampling frequency $F_e = 10\,\text{kHz}$ during 1 s with $\omega = 0.1534$ rad/s (supply frequency $f = 50\,\text{Hz}$) and $\omega_2 = 0.0307$ rad/s ($f_2 = 10\,\text{Hz}$). After HT demodulation, $\alpha = 10$ samples have been removed at the beginning and at the end of $|a_k(n)|$ to avoid edge effect problems. The fault index has been set to $\beta = 0.2$ to simulate faulty machine (see Figure 2.5 for time representation of $i_0(n)$).

2.7.3.1 Balanced system ($\psi = 0$)

For balanced system, the amplitude envelopes are the same for the three currents. Figures 2.6 and 2.7 display $|a(n)|$ and $|a_0(n)|$ extracted with CT, HT and TKEO, respectively, for a healthy and faulty cases. One can notice that the three demodulation techniques lead to the same envelope. Table 2.1 shows the values of the fault detector criteria σ_C^2, σ_H^2 and σ_{TKEO}^2 for faulty and healthy machine. The three criteria lead to similar results, indeed $\sigma_C^2 = \sigma_H^2 = \sigma_{TKEO}^2 = 0$ for healthy machine (i.e. $\beta = 0$)

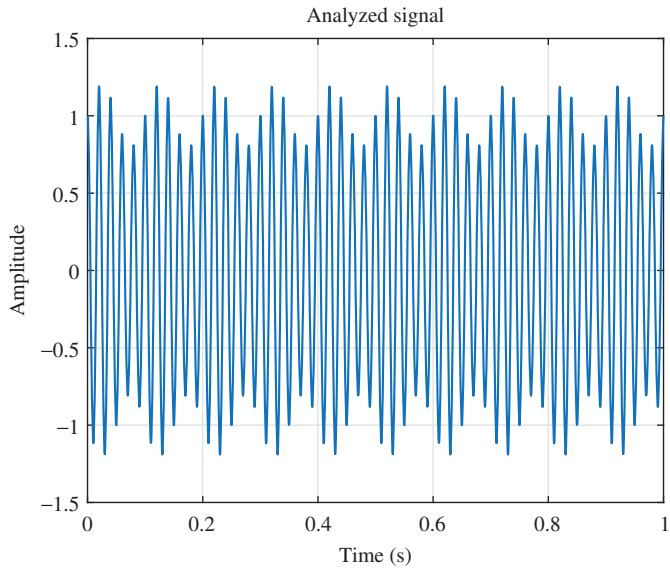

Figure 2.5 Time representation of the current $i_0(n)$ for a faulty machine ($\beta = 0.2$)

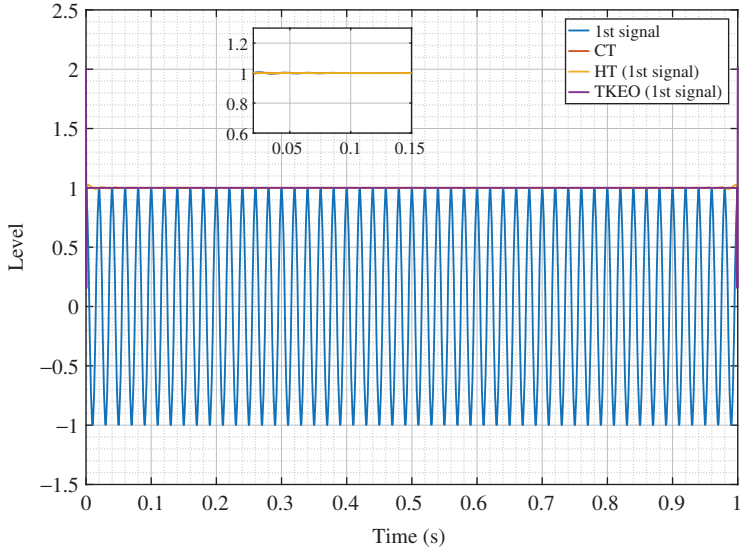

Figure 2.6 Balanced system healthy machine: time representation of the envelopes after CT, HT and TKEO demodulation ($\beta = 0$)

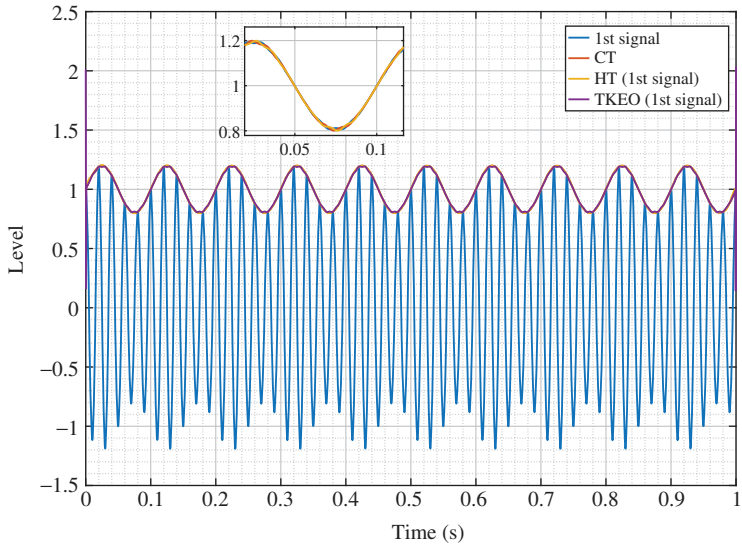

Figure 2.7 Balanced system faulty machine: time representation of the envelopes after CT, HT and TKEO demodulation ($\beta = 0.2$)

Table 2.1 Fault detector for healthy and faulty machines

System	Demodulation	Fault detector	
		Healthy case	**Faulty case**
Balanced and stationary	CT	$\sigma_C^2 = 0.000$	$\sigma_C^2 = 0.020$
	HT	$\sigma_H^2 = 0.000$	$\sigma_H^2 = 0.020$
	TKEO	$\sigma_{TKEO}^2 = 0.000$	$\sigma_{TKEO}^2 = 0.018$
Unbalanced and stationary	CT	$\sigma_C^2 = 0.000$	$\sigma_C^2 = 0.005$
	HT	$\sigma_H^2 = 0.000$	$\sigma_H^2 = 0.020$
	TKEO	$\sigma_{TKEO}^2 = 0.000$	$\sigma_{TKEO}^2 = 0.018$
Unbalanced and nonstationary	CT	$\sigma_C^2 = 0.000$	$\sigma_C^2 = 0.005$
	HT	$\sigma_H^2 = 0.001$	$\sigma_H^2 = 0.021$
	TKEO	$\sigma_{TKEO}^2 = 0.000$	$\sigma_{TKEO}^2 = 0.017$

and $\sigma_C^2 = \sigma_H^2 = \sigma_{TKEO}^2 = 0.020$ for faulty ones (i.e. $\beta = 0.2$). Therefore, a fault can be easily detected in this context by setting the threshold of the fault detector to $\gamma_C = \gamma_H = \gamma_{TKEO} = 0.010$. From a practical point of view, one should note that CT demodulation must be preferred for balanced system since it has a lower complexity than HT and TKEO and does not suffer from edge-effect problems.

2.7.3.2 Unbalanced system ($\psi_0 = 0, \psi_1 = 2\pi/3, \psi_2 = -2\pi/3$)

Let us simulate a system which is unbalanced under faulty condition. Figure 2.8 displays amplitude $a(n)$ and the envelope $|a_0(n)|$ extracted with CT, HT and TKEO respectively, for a faulty machine. As expected, CT is not able to demodulate the signals. Table 2.1 presents the values of the fault detector criterion σ_C^2, σ_H^2 and σ_{TKEO}^2 under healthy and faulty conditions. In our simulations, criterion σ_H^2 leads to the same values for balanced and unbalanced system whereas the value of σ_H^2 decreases under unbalanced condition. One can notice that the difference between healthy and faulty case is larger for σ_H^2. For fault detection, an hypothesis-test threshold equal to $\gamma_C = 0.0025$ for σ_C^2 and $\gamma_H = \gamma_{TKEO} = 0.010$ for σ_H^2 and σ_{TKEO}^2 lead to correct results in this context.

2.7.3.3 Unbalanced system ($\psi_0 = 0, \psi_1 = 2\pi/3, \psi_2 = -2\pi/3$) under nonstationary supply frequency

To simulate nonstationary environment, supply frequency f is assumed to vary linearly between 10 and 50 Hz, i.e.

$$\omega(n) = \frac{2\pi}{F_e}\left(\frac{40}{2N}n + 10\right) \tag{2.48}$$

Figure 2.9 displays amplitude $|a(n)|$ and the envelope $|a_0(n)|$ extracted with CT, HT and TKEO, respectively, for a faulty machine under nonstationary supply

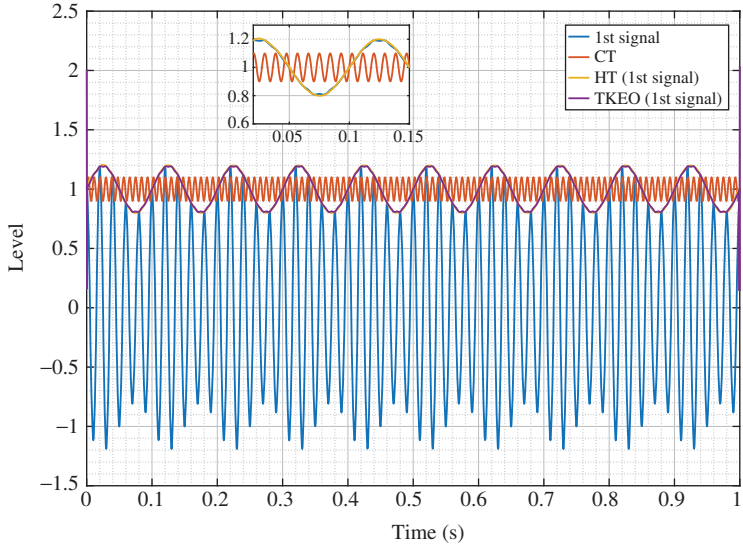

Figure 2.8 Unbalanced system faulty machine: time representation of the envelopes after CT, HT and TKEO demodulation ($\beta = 0.2$)

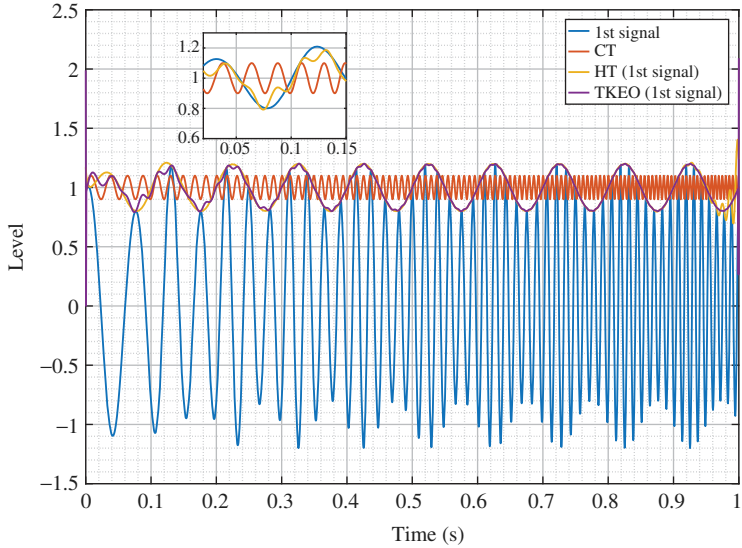

Figure 2.9 Non-balanced system under nonstationary condition—faulty machine: time representation of the envelopes after CT, HT and TKEO demodulation ($\beta = 0.2$)

frequency. As edge-effect problem occurs for HT (see Figure 2.9), α samples have been removed at the beginning and at the end of $|a_k(n)|$. Table 2.1 presents the values of the fault detector criterion σ_C^2, σ_H^2 and σ_{TKEO}^2. One should note that the values σ_C^2, σ_H^2 and σ_{TKEO}^2 do not depend on the stationary assumption in our context. Therefore, fault detectors based on amplitude demodulation seem to be well-suited for nonstationary scenario. In particular, these detectors do not need to employ complicated time-frequency representations (like spectrogram and Wigner–Ville) that suffer from artifact or poor resolution.

2.8 EMD method

Besides, in typical electric machines, stator current components are the supply fundamental, harmonics, additional components due to slot harmonics, saturation harmonics, other components from unknown sources such as environmental noise and design imperfection, and eventually effect introduced by bearing faults. In typical electric machines, the stator current is a multicomponets signal and can be expressed by a temporal model as

$$x(t) = \sum_{k=1}^{M} a_k(t) \sin(\phi_k(t)) \tag{2.49}$$

with $a_k(t) = a_k(1 + m_{ka} \sin(2\pi f_{ka} t + \varphi_{ka}))$ and $\phi_k(t) = 2\pi f_k t + m_{kp} \sin(2\pi f_{kp} t + \varphi_{kp})$. Here m_{ka} and m_{kp} are the AM index, and the PM index, respectively, that can be introduced by a fault as an AM/PM effect. This work considers only the AM effect. Therefore, $m_{kp} = 0$ and $\phi_k(t) = 2\pi f_k t$, where $f_k = k f_0$ with f_0 is the fundamental frequency and k is the harmonic order. Hence, for fault detection, a possible approach relies on the use of amplitude demodulation techniques to extract fault-related features. In this multicomponent signal context, the empirical mode decomposition (EMD) is considered. The EMD is an emerging signal processing algorithm for signal demodulation. It has been first introduced in [55], and has since become an established tool for the analysis of nonstationary and nonlinear data [56]. This approach has focused considerable attention and has been widely used for rotating machinery fault diagnosis [22,54,57,58]. It is an adaptive time-frequency data analysis method for nonlinear and nonstationary signals [55], and behaves like an adaptive filter bank [59]. Compared to FFT or wavelets that decompose a signal into a series of *sine* functions or scaled mother wavelet, the EMD decomposes the multicomponent signal into a series of mono-components signal, known as *intrinsic mode function* denoted *IMFs*, and based on the local characteristic time-scale of the signal. This decomposition can be described as follows:

- Identification of all extrema of the logged current;
- Interpolation between minima (respectively maxima) ending up with some envelope $e_{\min}(n)$ (respectively $e_{\max}(n)$);

- Computation of the mean:

$$R(n) = \frac{e_{\min}(n) + e_{\max}(n)}{2} \tag{2.50}$$

- Extraction of the detail:

$$d_m(n) = i(n) - R(n) \tag{2.51}$$

- Iteration on the residue $R(n)$

In practice, this algorithm has to be refined by a sifting process until the detail d_m can be considered as *IMF* [55]. To illustrate the EMD concept, let us assume the synthesized signal $x_{\text{syn}}(t)$ given by

$$x_{\text{syn}}(t) = a_1 \sin(\omega_1 t) + a_2 \sin(\omega_2 t), \tag{2.52}$$

where a_1 and a_2 are the amplitudes of the first and the second component respectively, while ω_1 and ω_2 are pulsations of those components. By decomposing $x_{\text{syn}}(t)$ through the EMD algorithm, the result is depicted in Figure 2.10. It appears clearly that the two components are presented by the first and second *IMFs*. Unfortunately, real signals

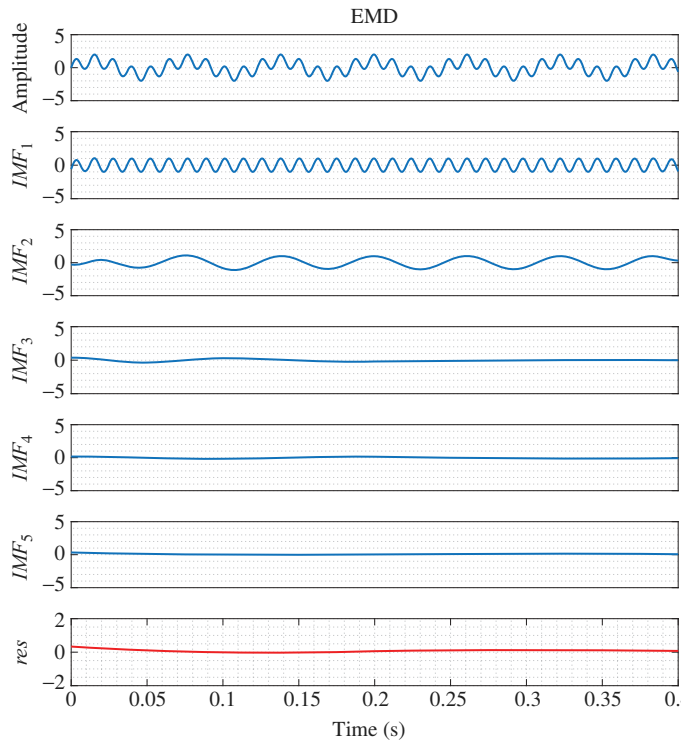

Figure 2.10 EMD for uncorrupted synthetic signal

are not immunized from noises, and in order to have a look on the behavior of the EMD on the added noise signal, let us consider that signal is corrupted by an added white Gaussian noise (AWGN), then $x_{\text{syn}}(t)$ can be expressed by

$$x_{\text{syn}}(t) = a_1 \sin(\omega_1 t) + a_2 \sin(\omega_2 t) + \text{AWGN}, \tag{2.53}$$

The corresponding local time oscillations or *IMFs* and residue are depicted in Figure 2.11.

The first observation is that the corresponding *IMFs* are shifted from the fourth to fifth *IMFs*; this is due to the AWGN to the original signal, hence high-frequency oscillations are introduced at the first, second and third *IMFs*. The second observation is the occurrence of the second component into at least two consecutive *IMFs*. This phenomenon is the mode mixing, as mentioned before. Consequently, it is difficult to really understand what the EMD provides as *IMFs*, and are devoid of a physical meaning [55]. Other drawbacks are indexed in literature, such as the *ad hoc* process on which it is based [59], sensitivity to noise, and the fact that it suffers from mode mixing. To overcome the mode-mixing problem, the Ensemble EMD (EEMD) was introduced.

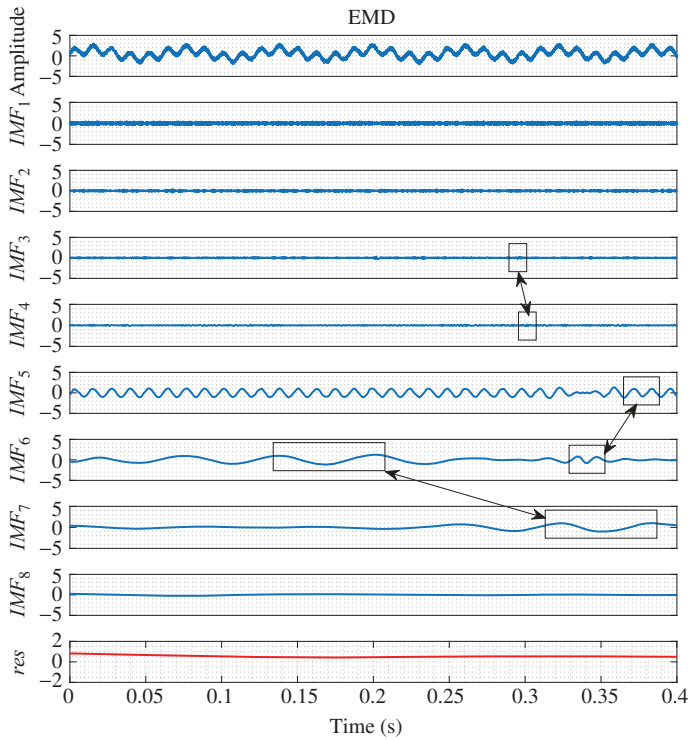

Figure 2.11 EMD for corrupted synthetic signal by an AWGN

2.9 Ensemble EMD principle

As mentioned next, the main drawbacks of the EMD are that it is based on an *ad hoc* process [59], it is mathematically difficult to model, it is noise sensitive and it suffers from mode mixing. Consequently, it is difficult to understand what the EMD provides as *IMFs* that are devoid from a physical meaning [55]. To deal with this drawbacks, an EEMD was proposed in [60,61], and has become a tool for the analysis of nonstationary and nonlinear data [56] in a wide of range applications in signal processing [62] and fault detection [22,57,58]. It is an improved EMD and is described as a noise-assisted data analysis method. Indeed, it deals with several EMD decompositions of the original signal corrupted by different artificial noises. The final EEMD is then the average of each EMD and defines true *IMFs* as the mean of an ensemble of trials. The EEMD algorithm is depicted in Figure 2.12 and its implementation is described step by step in [54].

The EEMD reliability depends on the choice of the ensemble number denoted by M and the add-noise amplitude a. These two parameters are linked by the following [60]:

$$e = \frac{a}{\sqrt{M}} \tag{2.54}$$

where e is the standard deviation error, and it is defined as the discrepancy between the input signal and the corresponding *IMF*.

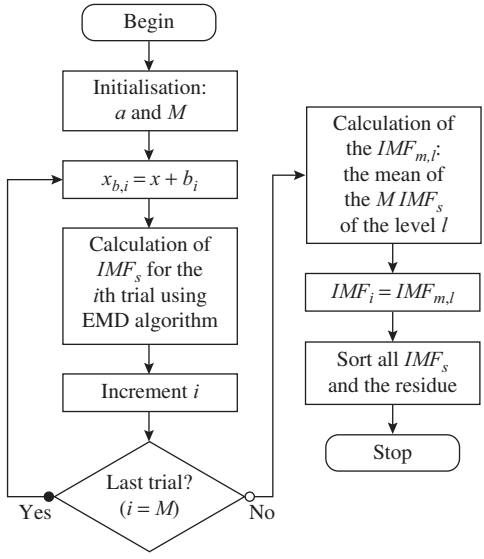

Figure 2.12 EEMD process for signal decomposition

So, through EEMD algorithm, a signal $x(t)$ can be expressed as a sum of k modes or *IMFs* as follows:

$$x(t) = \sum_{i=1}^{k} IMF_i(t) + res(t) \tag{2.55}$$

Figures 2.13 and 2.14 illustrate the decomposition of free-noise signal and corrupted signal, respectively.

Let us consider the series $x(n)\,(n = 1, \ldots, N)$ is the acquired stator current. Under the multicomponent assumption, the sampled current $x(n)$ can be decomposed as

$$x(n) = \sum_{i=1}^{j} IMF_i(n) + res(n) \tag{2.56}$$

where $IMF_i(n)$ is the ith intrinsic mode function, $res(n)$ is the residue and j the total number of *IMFs*. In practice, *IMFs* are unknown and must be extracted from the

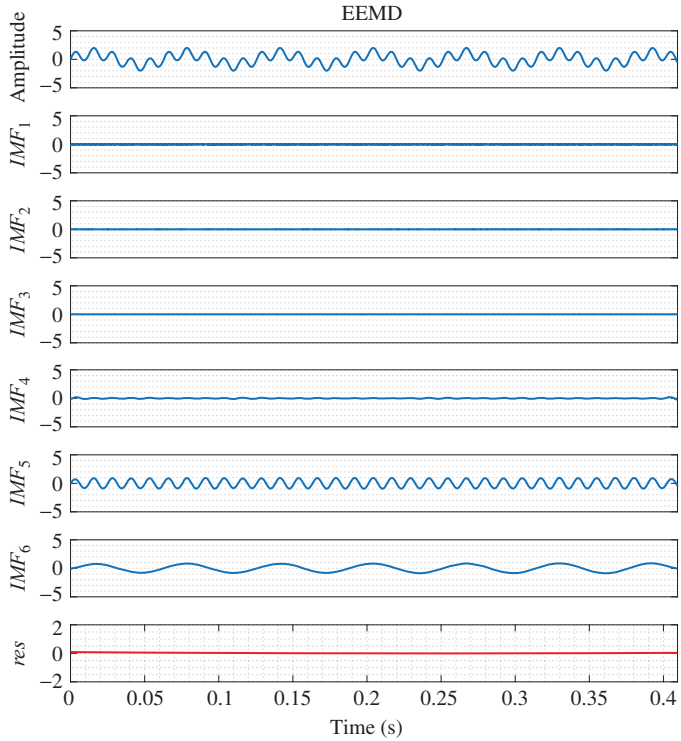

Figure 2.13 EEMD for uncorrupted synthetic signal

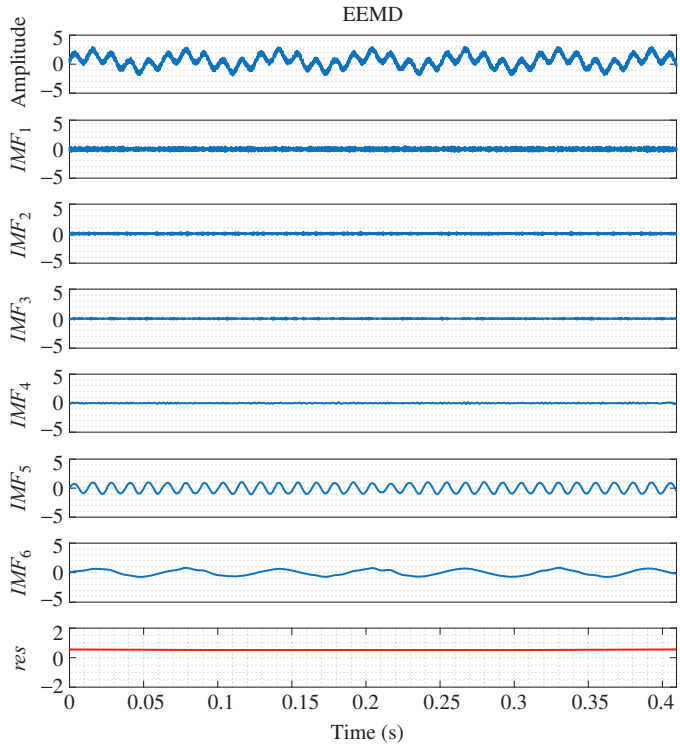

Figure 2.14 EEMD for corrupted synthetic signal by an AWGN

stator current $x(n)$. However, at least one *IMF* is related or representative of the main component. Consequently, $x(n)$ can be expressed by

$$x(n) = \sum_{i=1}^{c-1} IMF_i(n) + IMF_c(n) + \sum_{i=c+1}^{j} IMF_i(n) + res(n) \tag{2.57}$$

where $IMF_c(n)$ is the closest *IMF* to the original signal $x(n)$.

So, the main issue that rises is how to extract this *IMF*. To answer this question, in [63–65], a mode decomposition-based notch filter was developed.

2.10 EEMD-based notch filter

As mentioned in previous subsection, the decomposition of signal $x(t)$ through EEMD leads to a sum of modes as expressed in (2.57); among these modes, at least one mode is representative to the original signal, and this mode is the dominant mode denoted by $IMF_d(n)$. Assuming that the occurrence of a fault introduces a new component in the original signal, a specific mode denoted by IMF_e is introduced in the mode decomposition of this original signal.

The aim of the notch filter is to cancel the dominant *IMF*, and the result denoted by $x(n)_{c_{EEMD}}$ can therefore be used to detect bearing failure.

2.10.1 Statistical distance measurement

The statistical distance quantifies the distance between two statistical quantities, which can be two random variables, or two probability distributions or samples. Various approaches have been indexed in statistics literature and investigated in various fields, particularly for fault detection and diagnostic [54,66]. The statistical tool known as Pearson's correlation is used to measure the distance, and to give a weight to dependency between two temporal series $x(n)$ and $y(n)$ [67]. This dependency is weighted by a coefficient denoted by $r(x,y)$ and defined by (2.58); a value of this coefficient close to -1 or 1 indicates that $x(n)$ and $y(n)$ are highly correlated positively or negatively, respectively, while a value around 0 indicates that there is no dependency between $x(n)$ and $y(n)$ [65].

$$r(x,y) = \frac{\sum_n [(x(n) - m_x) * (y(n) - m_y)]}{\sqrt{\sum_n (x(n) - m_x)^2} \cdot \sqrt{\sum_n (y(n) - m_y)^2}} \tag{2.58}$$

where m_x and m_y are the means of x and y, respectively.

2.10.2 Dominant-mode cancellation

The cancelation of the dominant *IMF* is illustrated in Figure 2.15.

The algorithm for the cancellation of the dominant *IMF* can be sketched as consisting of three steps [65]:

- Step 1: The analyzed signal is decomposed into a set of *IMFs* through EEMD,
- Step 2: Pearson's correlation coefficient is calculated using (2.58) as many times as there are *IMFs* then $r_d \approx 1$ indexes the IMF_d,
- Step 3: Then, the indexed IMF_d is removed from the analyzed signal $x(n)$ and the result denoted by $x(n)_{dEEMD}$ can therefore be used to detect bearing failure.

To measure the strength of the association between two variables using the Pearson's correlation, let us consider $X(n)$ as line current and $Y(n)$ as the *IMF*, so

$$X(n) = x(n) \tag{2.59}$$

and

$$Y_i(n) = IMF_i(n) \tag{2.60}$$

or

$$Y_i(n) = Mode_i(n) \tag{2.61}$$

where $(i = 1, \ldots, j)$ corresponds to the *IMF* rank and j is the total number of *IMFs*. Then, the Pearson's correlation coefficient r_i is computed for each pair $(X(n), Y_i(n))$; as result, the score $r_d \approx 1$ indexes the dominant *IMF* denoted by IMF_d. After determining

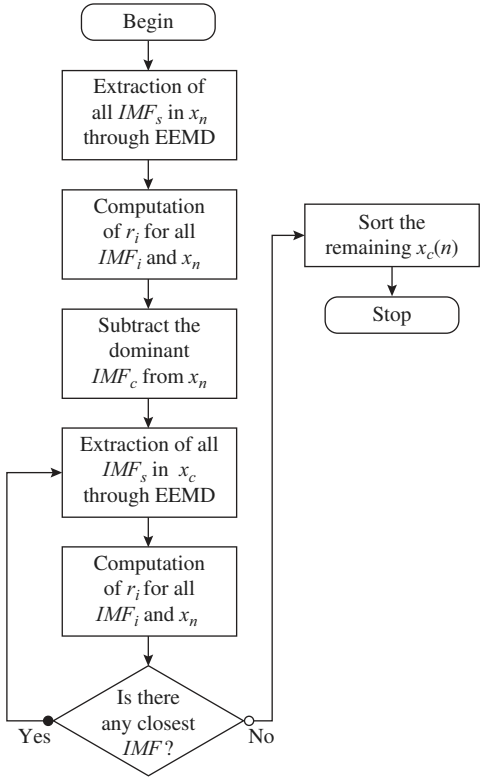

Figure 2.15 Closest IMF subtraction principle [54]

the IMF_d, it is canceled from the original signal $x(n)$, and the remaining signal $x_c(n)$ expressed by (2.62) can be investigated for bearing failure detection.

$$x_{c_{EEMD}}(n) = x(n) - IMF_d(n), \tag{2.62}$$

The cancellation process is repeated until there is no correlation between the main signal $x(n)$ and the *IMFs* contained in $x_c(n)$.

2.10.3 Fault detector based on EEMD demodulation

As mentioned previously for CT, HT and TKEO, the variance of $x_c(n)$ is investigated as a fault detector. This statistics criterion, denoted by σ^2, measures the deviation of the amplitude around its mean μ. It is given by

$$\sigma^2 = \frac{1}{N}\sum_{n=0}^{N-1}(x_c(n) - \mu)^2 \tag{2.63}$$

where μ is the average of $x_c(n)$. To avoid the EEMD edge-effect problem, $x_c(n)$ is then truncated by removing α samples at the beginning and at the end of $x_c(n)$. Hence, the

proposed criterion σ^2 is expressed by the following [68]:

$$\sigma^2 = \frac{1}{(N-2\alpha)} \left(\sum_{n=\alpha}^{N-\alpha-1} (x_c(n) - \mu)^2 \right) \tag{2.64}$$

and

$$\mu = \frac{1}{(N-2\alpha)} \sum_{n=\alpha}^{N-\alpha-1} x_c(n) \tag{2.65}$$

The hypothesis test to detect a fault can therefore be formulated as follows: If $\sigma^2 > \gamma$, the machine is faulty, where γ is a threshold. For ideal acquisition conditions $\gamma = 0$, but in real-world applications there is always an add noise to measurements, then γ can be set subjectively.

2.10.4 Synthetic signals

In this validation step, simulations have been performed with AM synthetic signals. According to (2.49), and since additional components could be considered as noise in the context of bearing faults detection [69], the AM synthetic signal corrupted by an additive noise δ is defined as

$$x(n) = \underbrace{(1 + \beta \sin(\omega_2 n + \psi))}_{a(n)} \cdot \cos(\omega n + \phi) + \delta(n). \tag{2.66}$$

where $n = 0, \ldots, N-1$ is the sample index, N being the number of samples, and ϕ is the phase parameter. In (2.66), frequency ω is equal to $2\pi f/F_e$ and ω_2 is equal to $2\pi f_2/F_e$ (where f, f_2 and F_e are the supply, fault and sampling frequency, respectively) and amplitude $a(n)$ is related to the fault. It should be noted that the additive noise $\delta(n)$ is supposed to be a zero mean and Gaussian noise process. This assumption is an approximation of the electrical noise picked up in the wiring and signal conditioning circuits [70], and it is widely considered in the measurement and electrical engineering communities [71]. The modulation index β is the fault index, then $\beta = 0$ is for the healthy case and $\beta > 0$ is for the faulty one. Simulations have been carried out with a sampling frequency $F_e = 10\,\text{kHz}$, a supply frequency $f = 50\,\text{Hz}$ and $f_2 = 100\,\text{Hz}$. In order to simulate healthy and faulty cases, the modulation index has been set, respectively, to $\beta = 0.0$ for healthy case, and $\beta = 0.1$, 0.15 and 0.2 for different severity of the fault (Figure 2.16).

Figures 2.17 and 2.18 show the EEMD result of the synthetic signal $x(n)$ for both healthy and faulty cases, respectively.

It clearly shows that at least one *IMF* is close to the original signal. In order to quantify the strength of the association between $x(n)$ and each *IMF*, the Pearson's correlation coefficient r_i is computed and results are depicted in Table 2.2. In this case, IMF_5 is the closest to the main signal. It is then subtracted, and the variance

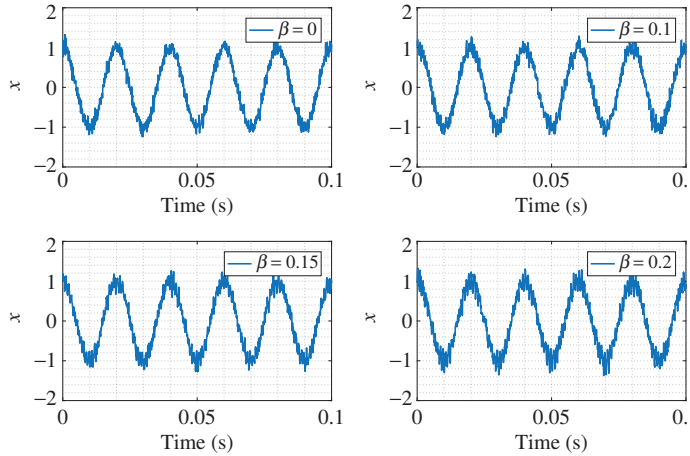

Figure 2.16 Time representation of the synthetic signal for different modulation index

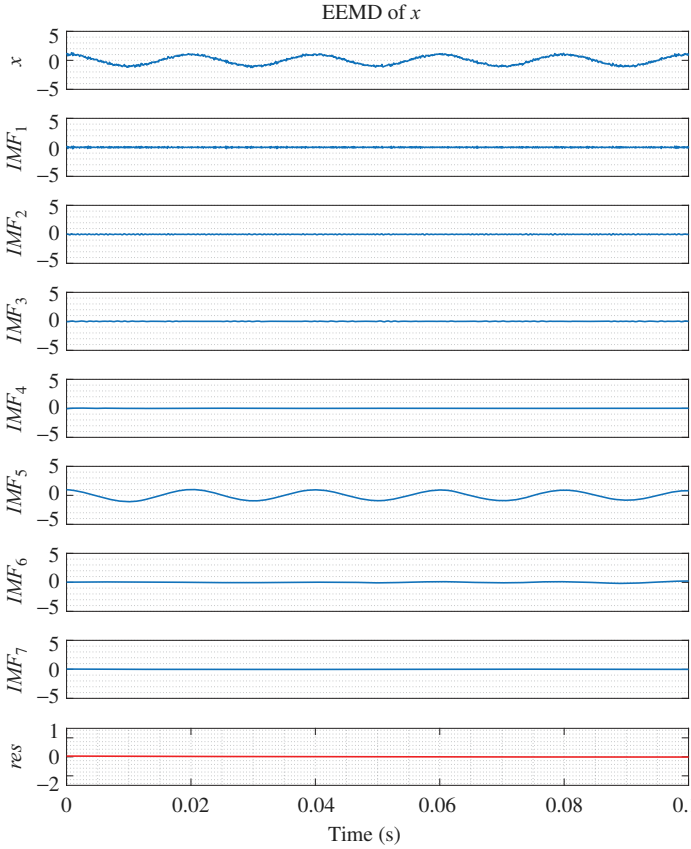

Figure 2.17 EEMD for modulated synthetic signal: $\beta = 0$

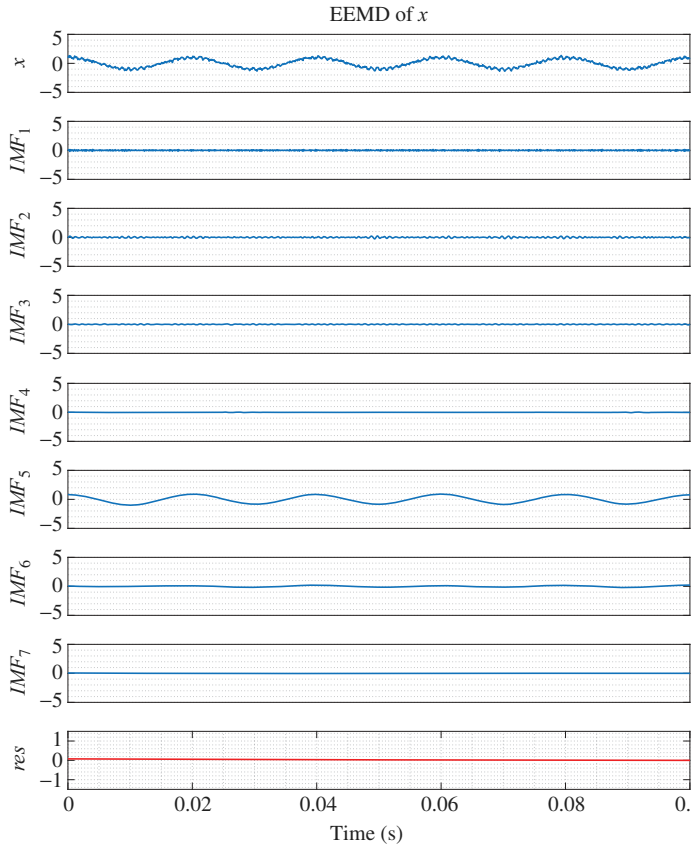

Figure 2.18 EEMD for modulated synthetic signal: $\beta = 0.2$

Table 2.2 Coefficients of Pearson's correlation of synthetic signal for EEMD

IMF rank	$\boldsymbol{\beta = 0.0}$	$\boldsymbol{\beta = 0.1}$	$\boldsymbol{\beta = 0.15}$	$\boldsymbol{\beta = 0.2}$
IMF_1	0.1129	0.1182	0.1189	0.1193
IMF_2	0.0873	0.1143	0.1324	0.1543
IMF_3	0.0688	0.0811	0.1141	0.1387
IMF_4	0.0598	0.0583	0.0284	0.0493
IMF_5	0.9883	0.9820	0.9825	0.9771

of the remaining signal is computed and results for both algorithms are presented in Table 2.2. It is clearly shown that the fault criterion σ^2 rises with the modulation index β, as presented in Table 2.3. For healthy case ($\beta = 0$) and due to the added noise $\delta(n)$, σ^2 is not equal to 0.

Table 2.3 The variance (σ^2) of x_c for EEMD

$\beta = 0.0$	$\beta = 0.1$	$\beta = 0.15$	$\beta = 0.2$
$\sigma^2 = 0.0044$	$\sigma^2 = 0.0057$	$\sigma^2 = 0.0067$	$\sigma^2 = 0.0076$

2.11 Summary and conclusion

In this chapter, we have proposed a review on fault detection based on demodulation techniques. First, the motor currents are demodulated using CT, HT and TKEO. Then, a hypothesis test based on the statistical variance of the demodulated envelope is performed to discriminate between healthy and faulty machines. The results of several simulations have shown that the mentioned methods perform well in stationary and nonstationary scenarios. Furthermore, results have shown that, even if CT is computationally attractive compared to HT and TKEO, this low-complexity demodulation technique can be inappropriate for the diagnosis of unbalanced system, and CT, HT and TKEO are inappropriate for multicomponent signals. Second, for multicomponent signals, the EMD-based notch filter is described; the core of this notch filter is a data-driven strategy combined to a statistical tool. The filtering operation was carried out following three steps: the first step concerns the decomposition of the phase machine current into *IMFs* using EEMD, then at the second step the dominant mode is subtracted from the original signal, and finally in the last step relays on the use of a statistical feature as a fault detector. The results of several simulations have shown that the proposed method performs well for amplitude-modulated signal regardless of the mode rank.

References

[1] Cardoso AJM. Diagnosis and Fault Tolerance of Electrical Machines, Power Electronics and Drives. The Institution of Engineering and Technology, United Kingdom. IET Energy Engineering; 2018.

[2] Thorsen OV and Dalva M. Failure identification and analysis for high-voltage induction motors in the petrochemical industry. IEEE Transactions on Industry Applications. 1999;35(4):810–818.

[3] Thomson WT and Stewart ID. Online current monitoring for fault diagnosis in inverter-fed induction motors. In: Third International Conference on Power Electronics and Variable-Speed Drives; 1988. pp. 432–435.

[4] Kliman GB, Koegl RA, Stein J, Endicott RD, and Madden MW. Noninvasive detection of broken rotor bars in operating induction motors. IEEE Transactions on Energy Conversion. 1988;3(4):873–879.

[5] Antonino-Daviu J, Corral-Hernandez J, Climente-Alarcò V, *et al.* Case stories of advanced rotor assessment in field motors operated with soft-starters and frequency converters. In: IECON 2015—41st Annual Conference of the IEEE Industrial Electronics Society; 2015. pp. 001139–001144.

[6] Frosini L, Harlişca C and Szabó L. Induction machine bearing fault detection by means of statistical processing of the stray flux measurement. IEEE Transactions on Industrial Electronics. 2015;62(3):1846–1854.
[7] Seera M and Lim CP. Online motor fault detection and diagnosis using a hybrid FMM-CART model. IEEE Transactions on Neural Networks and Learning Systems. 2014;25(4):806–812.
[8] Leite VCMN, da Silva JGB, Veloso GFC, *et al.* Detection of localized bearing faults in induction machines by spectral kurtosis and envelope analysis of stator current. IEEE Transactions on Industrial Electronics. 2015;62(3):1855–1865.
[9] Benbouzid MEH. A review of induction motors signature analysis as a medium for faults detection. IEEE Transactions on Industrial Electronics. 2000;47(5):984–993.
[10] Zhang P, Du Y, Habetler TG, *et al.* A survey of condition monitoring and protection methods for medium-voltage induction motors. IEEE Transactions on Industry Applications. 2011;47(1):34–46.
[11] Wang W and Jianu OA. A smart sensing unit for vibration measurement and monitoring. IEEE/ASME Transactions on Mechatronics. 2010;15(1):70–78.
[12] Tavner P, Ran L, Penman J, and Sedding H. Condition Monitoring of Rotating Electrical Machines. IET Power and Energy series. IET, London; 2008.
[13] Schoen RR, Habetler TG, Kamran F, *et al.* Motor bearing damage detection using stator current monitoring. IEEE Transactions on Industry Applications. 1995;31(6):1274–1279.
[14] Frosini L, Harlişca C and Szabó L. Stator current and motor efficiency as indicators for different types of bearing fault in induction motor. IEEE Transactions on Industrial Electronics. 2010;57(1):244–251.
[15] Ibrahim A, Badaoui ME, Guillet F, *et al.* A new bearing fault detection method in induction machines based on instantaneous power factor. IEEE Transactions on Industrial Electronics. 2008;55(12):4252–4259.
[16] Elbouchikhi E, Choqueuse V and Benbouzid MEH. Induction machine faults detection using stator current parametric spectral estimation. Mechanical Systems and Signal Processing. 2015;52–53:447–464.
[17] Kia SH, Henao H and Capolino GA. A high-resolution frequency estimation method for three-phase induction machine fault detection. IEEE Transactions on Industrial Electronics. 2007;54(4):2305–2314.
[18] Stoica P and Moses R. Introduction to Spectral Analysis. Prentice Hall, Upper Saddle River, New Jersey; 1997.
[19] Elbouchikhi E, Choqueuse V and Benbouzid M. Induction machine bearing faults detection based on a multi-dimensional MUSIC algorithm and maximum likelihood estimation. ISA Transactions. 2016;63:413–424.
[20] Blodt M, Bonacci D, Regnier J, *et al.* On-line monitoring of mechanical faults in variable-speed induction motor drives using the Wigner distribution. IEEE Transactions on Industry Applications. 2008;55(2):522–533.
[21] Blodt M, Regnier J and Faucher J. Distinguishing load torque oscillations and eccentricity faults in induction motors using stator current Wigner distributions. IEEE Transactions on Industry Applications. 2009;45(6):1991–2000.

[22] Antonino-Daviu JA, Riera-Guasp M, Pineda-Sanchez M, *et al.* A critical comparison between DWT and Hilbert-Huang-based methods for the diagnosis of rotor bar failures in induction machines. IEEE Transactions on Industry Applications. 2009;45(5):1794–1803.

[23] Cusido JC, Romeral L, Ortega JA, *et al.* Fault detection in induction machines using power spectral density in wavelet decomposition. IEEE Transactions on Industrial Electronics. 2008;55(2):633–643.

[24] Riera-Guasp M, Antonio-Daviu JA, Roger-Folch J, and Molina Palomares MP. The use of the wavelet approximation signal as a tool for the diagnosis of rotor bar failure. IEEE Transactions on Industry Applications. 2008;44(3):716–726.

[25] Kia SH, Henao H and Capolino GA. Diagnosis of broken-bar fault in induction machines using discrete wavelet transform without slip estimation. IEEE Transactions on Industry Applications. 2009;45(4):1395–1404.

[26] Mandic DP, ur Rehman N, Wu Z, *et al.* Empirical mode decomposition-based time-frequency analysis of multivariate signals: the power of adaptive data analysis. IEEE Signal Processing Magazine. 2013;30(6):74–86.

[27] Tavner PJ. Review of condition monitoring of rotating electrical machines. IET Electric Power Applications. 2008;2(4):215–247.

[28] Stack JR, Harley RG and Habetler TG. An amplitude modulation detector for fault diagnosis in rolling element bearings. IEEE Transactions on Industrial Electronics. 2004;51(5):1097–1102.

[29] Riley CM, Lin BK, Habetler TG, *et al.* A method for sensorless on-line vibration monitoring of induction machines. IEEE Transactions on Industry Applications. 1998;34(6):1240–1245.

[30] Elbouchikhi E, Choqueuse V and Benbouzid MEH. Condition monitoring of induction motors based on stator currents demodulation. International Review on Electrical Engineering. 2015;10(6):1–6.

[31] Boualem B. Chapter 1. Time-frequency and instantaneous frequency concepts. In: Time-frequency Signal Analysis and Processing. 2nd ed. Academic Press, Oxford; 2016. pp. 31–63.

[32] Boashash B. Estimating and interpreting the instantaneous frequency of a signal. II. Algorithms and applications. Proceedings of the IEEE. 1992;80(4): 540–568.

[33] Delprat N, Escudie B, Guillemain P, *et al.* Asymptotic wavelet and Gabor analysis: extraction of instantaneous frequencies. IEEE Transactions on Information Theory. 1992;38(2):644–664.

[34] IEEE. IEEE Standard Definitions for the Measurement of Electric Power Quantities under Sinusoidal, Nonsinusoidal, Balanced, or Unbalanced Conditions. IEEE Press; 2010.

[35] Trajin B, Chabert M, Regnier J, *et al.* Hilbert versus Concordia transform for three-phase machine stator current time-frequency monitoring. Mechanical Systems & Signal Processing. 2009;23(8):2648–2657.

[36] Onel IY and Benbouzid MEH. Induction motor bearing failure detection and diagnosis: Park and Concordia transform approaches comparative study. IEEE/ASME Transactions on Mechatronics. 2008;13(2):257–262.

[37] Cruz SMA and Cardoso AJM. Stator winding fault diagnosis in three-phase synchronous and asynchronous motors, by the extended Park's vector approach. IEEE Transactions on Industry Applications. 2001;37(5): 1227–1233.

[38] Cardoso AJM, Cruz SMA and Fonseca DSB. Inter-turn stator winding fault diagnosis in three-phase induction motors, by Park's vector approach. IEEE Transactions on Energy Conversion. 1999;14(3):595–598.

[39] Cardoso AJM and Saraiva S. Computer-aided detection of airgap eccentricity in operating three-phase induction motors by Park's Vector Approach. IEEE Transactions on Industry Applications. 1993;28(5):897–901.

[40] Cizek V. Discrete Hilbert transform. IEEE Transactions on Audio and Electroacoustics. 1970;18(4):340–343.

[41] Gabor D. Theory of communication. Journal Institution of Electrical Engineers London. 1996;93(3):429–457.

[42] Oppenheim AV, Schafer RW and Padgett WT. Discrete-Time Signal Processing. 3rd ed. Prentice Hall, Upper Saddle River, New Jersey; 2009.

[43] Maragos P, Kaiser J and Quartieri T. On amplitude and frequency demodulation using energy operators. IEEE Transactions on Signal Processing. 1993;41(4):1532–1550.

[44] Maragos P, Kaiser J and Quatieri T. Energy separation in signal modulations with application to speech analysis. IEEE Transactions on Signal Processing. 1993;10(41):3024–3051.

[45] Nejjari H and Benbouzid MEH. Monitoring and diagnosis of induction motors electrical faults using a current Park's vector pattern learning approach. IEEE Transactions on Industry Applications. 2000;36(3):730–735.

[46] Jaksch I. Fault diagnosis of three-phase induction motors using envelope analysis. In: Proceedings of SDEMPED. Atlanta, USA; 2003. pp. 289–293.

[47] Diallo D, M E H Benbouzid DH and Pierre X. Fault detection and diagnosis in an induction machine drive: a pattern recognition approach based on Concordia stator mean current vector. IEEE Transactions on Energy Conversion. 2005;20(3):512–519.

[48] Ocak H and Loparo KA. A new bearing fault detection and diagnosis schema based on hidden Markov modeling of vibration signals. In: Proceedings of IEEE International Conference on Acoustics, Speech, and Signal Processing (ICASSP). Salt Lake City, USA; 2001. pp. 3141–3144.

[49] Miao Q and Makis V. Condition monitoring and classification of rotating machinery using wavelets and hidden Markov models. Mechanical Systems and Signal Processing. 2007;21(2):840–855.

[50] Guo L, Chen J and Li X. Rolling bearing fault classification based on envelope spectrum and support vector machine. Journal of Vibration and Control. 2009;15(9):1349–1363.

[51] Saidi L, Ali JB, Bechhoefer E, *et al.* Wind turbine high-speed shaft bearings health prognosis through a spectral Kurtosis-derived indices and SVR. Applied Acoustics. 2017;120:1–8.

[52] Yang W, Tavner PJ, Crabtree CJ, *et al.* Cost-effective condition monitoring for wind turbines. IEEE Transactions on Industrial Electronics. 2010;57(1): 263–271.
[53] Kusiak A. Renewables: share data on wind energy. Nature. 2016;522(1): 19–21.
[54] Amirat Y, Benbouzid MEH, Wang T, *et al.* EEMD-based notch filter for induction machine bearing faults detection. Applied Acoustics. 2018;133: 202–209. Available from: http://www.sciencedirect.com/science/article/pii/S0003682X17308125.
[55] Huang NE, Shen Z, Long SR, *et al.* The empirical mode decomposition and Hilbert spectrum for nonlinear and nonstationary time series analysis. Proceedings of Royal Society, London. 1998;454:903–995.
[56] Tanaka T and Mandic DP. Complex empirical mode decomposition. IEEE Letters on Signal Processing. 2007;14(2):101–104.
[57] Yu D, Cheng J and Yang Y. Application of EMD method and Hilbert spectrum to the fault diagnosis of roller bearings. Mechanical Systems and Signal Processing. 2005;19(2):259–270.
[58] Amirat Y, Choqueuse V and Benbouzid MEH. EEMD-based wind turbine bearing failure detection using the generator stator current homopolar component. Mechanical Systems and Signal Processing. 2013;41(1):667–678.
[59] Gilles J. Empirical wavelet transform. IEEE Transactions on Signal Processing. 2013;61(16):3999–4010.
[60] Wu ZH and Huang NE. Ensemble empirical mode decomposition: a noise-assisted data analysis method. Advances in Adaptive Data Analysis. 2009;1: 1–41.
[61] Torres ME, Colominas MA, Schlotthauer G, *et al.* A complete ensemble empirical mode decomposition with adaptive noise. In: Proceedings of 2011 IEEE International Conference on Acoustics, Speech and Signal Processing (ICASSP); 2011. pp. 4144–4147.
[62] Huang NE and Shen SSP. Hilbert-Huang Transform and Its Applications. 2nd ed. World Scientific, Interdisciplinary Mathematical Sciences, Singapore; 2014.
[63] Amirat Y, Benbouzid MEH, Wang T, *et al.* Bearing fault detection in wind turbines using dominant intrinsic mode function subtraction. In: Proceedings of the 2016 IEEE IECON. (Florence) Italy; 2016. pp. 6961–6965.
[64] Amirat Y, Elbouchikhi E, Zhou Z, *et al.* Variational mode decomposition-based notch filter for bearing faults detection. In: Proceedings of the 2019 IEEE IECON. (Lisbon) Portugal; 2019. pp. 1–6.
[65] Amirat Y, Elbouchikhi E, Delpha C, *et al.* Chapter 4. Modal decomposition for bearing fault detection. In: Electrical Systems 1: From Diagnosis to Prognosis. John Wiley & Sons, Ltd, London; 2020. pp. 121–168. Available from: https://onlinelibrary.wiley.com/doi/abs/10.1002/9781119720317.ch4.
[66] Harmouche J, Delpha C and Diallo D. Improved fault diagnosis of ball bearings based on the global spectrum of vibration signals. IEEE Transactions on Energy Conversion. 2015;30(1):376–383.

[67] Proakis JG and Manolakis DG. Digital Signal Processing. 3rd ed. Prentice Hall, Upper Saddle River, New Jersey; 1996.
[68] Amirat Y, Choqueuse V and Benbouzid M. Condition monitoring of wind turbines based on amplitude demodulation. In: 2010 IEEE Energy Conversion Congress and Exposition; 2010. pp. 2417–2421.
[69] Zhou W, Habetler TG and Harley RG. Bearing fault detection via stator current noise cancellation and statistical control. IEEE Transactions on Industrial Electronics. 2008;55(12):4260–4269.
[70] Phadke AG. Synchronized phasor measurements—a historical overview. In: IEEE/PES Transmission and Distribution Conference and Exhibition. vol. 1; 2002. pp. 476–479.
[71] Komaty A, Boudraa AO, Augier B, *et al.* EMD-based filtering using similarity measure between probability density functions of IMFs. IEEE Transactions on Instrumentation and Measurement. 2014;63(1):27–34.